MODIFIED ENTHALAY METHOD APPLIED TO LASER ANNEALING OF SEMI CONDUCTOR FILMS

A. A. Rostami

Department of Mechanical Engineering
Isfahan University of Technology
Isfahan, Iran

C. P. Grigoropoulos

Department of Mechanical Engineering
University of California
Berkeley, CA 94720
USA

Abstract The rapid melting of silicon film due to the absorption of a CW laser beam radiation is studied. The silicon film melting and recrystallization is mainly controlled by the temperature distribution in the semiconductor. The enthalpy technique for the solution of phase change problems is used in an explicit finite difference form to calculate the transient temperature distribution in the silicon film and the substrate and the growth rates of the melt pool. The technique is modified so that it is not necessary to assign a constant temperature, Tm, to the mesh element that contains the melt front. Calculations are carried out for a range of laser beam parameters and material translational speeds. The results for the melt pool size are compared with the experimental data and reasonable agreement is obtained.

Key Words Phase Change, Melting, Solidification, Silicon Film, Laser Melting

چکیده ذوب سریع لایه سیلیکون در اثر جذب اشعه لیزر CW مورد مطالعه قرار گرفته است. ذوب و انجماد لایه سیلیکون شدیداً تحت کنترل توزیع دما در نیمه هادی است. برای تعیین توزیع دمای غیر دائم در لایه سیلیکون و لایه زیرین آن و همچنین ابعاد حوضچه مذاب از روش انتالپی بانضمام روش اختلاف محدود صریح استفاده شده است. در روش انتالپی اصلاحاتی به عمل آمد که نیازی نباشد که دمای ثابت نقطه ذوب T_m با المان شامل دوفاز جامد و مایع نسبت داد. محاسبات برای تعدادی از پارامترهای اشعه لیزری و سرعتهای مختلف حرکت افقی ماده انجام شده است. نتایج ابعاد حوضچه مذاب با نتایج تجربی مقایسه شده و دقت آن معقول بنظر می رسد.

INTRODUCTION

The silicon microfabrication has grown rapidly during the past several years. Examples of such advancements are microsensors, microactuators and other microdevices. Recrystallization of semiconductor films deposited on amorphous substrates has been shown to improve the transport properties and the reliability of electronic devices [1].

The use of light sources and, in particular, lasers to melt and subsequently recrystallize thin semiconductor layers on insulators, such as oxidized wafers and bulk substrates has shown good potential for applications to commercial technology [2]. Despite significant progress that has been made toward improving the crystal growth in thin silicon films, it has not been possible to consistently eliminate the formation of grain boundaries in the recrystallized material. These grain boundaries limit the use of the material as an active component in electronic devices

[1,3].

The crystal growth in silicon film melting and solidification is mainly controlled by the temperature distribution inside the film. The temperature distribution itself is controlled by the laser beam total power, the lateral distribution of the beam intensity and the translational speed of the target material. Experimental studies [4,5] have shown some success in controlling crystal growth by modifying the laser beam shape, and thus the induced temperature field. Reliable prediction of the temperature distribution in the thin film is essential for improving the electrical and crystalline properties by laser annealing. Extensive reviews of analytical and numerical techniques have been compiled [6,7,8,9]. The steady state temperature distribution in the melting of a thick silicon slab by a laser source has been given by Kokorowski [10]. The conventional enthalpy formulation of phase change problems along with simplifying assumptions has been used to obtain the transient temperature distribution for stationary thick slab irradiated by laser beam [11]. One-dimensional phase change finite difference models have been developed to study the effects of laser beam scanning rates and encapaulating structural configurations [12,13]. A three-dimensional transient numerical algorithm for thin silicon laser melting and recrystallization has been based on the conventional enthalpy method [15,16]. The numerical results were compared with sufficient experimental data and reasonable agreement was obtained [17].

In this study an explicit finite difference scheme incorporating the enthalpy formulation was employed to calculate the temperature distributions in the structure and the location of the solid-liquid interface in a thin silicon film deposited on a glass substrate.

During melting only a portion of the net energy transferred to a mesh element is consumed to phase change and the rest builds the sensible energy. The conventional enthalpy method was modified by implementing and extending previous work [18] to account for this effect. This energy balance modification improves the numerical method.

The problem studied in this work is one of three-dimensional heat transfer involving melting of a silicon film on top of a glass substrate covered by a thin encapsulating SiO_2 layer. The target is irradiated by a laser beam of specified temporal and spatial distributions of intensity. The variation with temperature of the thermophysical and optical properties of the target material is included in the calculations. The changes in these properties upon melting of the silicon film are also accounted for. The numerical model captures experimental trends and reasonable agreement is obtained between numerical results and experimental data.

PROBLEM FORMULATION

A polysilicon film of thickness d_{si} is deposited on a fused silica substrate of thickness d_{su}. The film is covered by a SiO_2 layer of thickness d_{cap}. A laser beam of Gaussian intensity distribution passes through the substrate, and is partially absorbed by the silicon film. The encapsulating layer and the substrate are transparent for the wavelengths of the multiline Argon ion laser beam, which is the annealing source considered in this work.

Convection and radiation losses from the top and bottom surfaces of the structure are accounted for. The target may travel at a speed, V, in the x-direction. The lateral dimensions of the structure are much larger than the thermal diffusion length of the materials corresponding to the time required to reach the quasi-steady conditions; hence an infinite computational domain is assumed in the x and y directions. On the other hand, the thickness of the silicon film and of the capping layer (0.5 μm each) are much smaller than the typical thermal diffusion length, so that temperature variations in the z-direction in these

layers may be neglected. However this is not true for the substrate which is 0.5mm thick.

Computational results obtained by treating the three layers separately showed that the temperature difference between the modpoints of the silicon film and the capping layer at the center of the beam did not exceed lK, except for very short time after the heating is started. These two layers were therefore considered as lumped for computational purpose. Thus, it is possible to use larger time intervals and reduce the computing time considerably, without any significant loss of numerical accuracy. The heat conduction equation in region 1, the lumped layers, may be written as

$$(\rho c_p)_1 \left(\frac{\partial T_1}{\partial t} + V\frac{\partial T_1}{\partial x}\right) = \frac{\partial}{\partial x}\left(k_1\frac{\partial T_1}{\partial x}\right) + \frac{\partial}{\partial y}\left(k_1\frac{\partial T_1}{\partial y}\right) + \frac{q_{abs} - (q_{rad} + q_{cv} + q_{cd})}{d} \qquad (1)$$

where $d = d_{si} + d_{cap}$. The target is assumed to travel in the x-direction. The heat conduction equation in the substrate is

$$(\rho c_p)_2 \left(\frac{\partial T_2}{\partial t} + V\frac{\partial T_2}{\partial x}\right) = \frac{\partial}{\partial x}\left(k_2\frac{\partial T_2}{\partial x}\right) + \frac{\partial}{\partial y}\left(k_2\frac{\partial T_2}{\partial y}\right) + \frac{\partial}{\partial z}\left(k_2\frac{\partial T_2}{\partial z}\right) \qquad (2)$$

The boundary conditions are

$$x \to \pm\infty, \quad T_1 = T_2 = T_\infty$$
$$y \to \pm\infty, \quad T_1 = T_2 = T_\infty$$
$$z = d, \quad T_1 = T_2$$
$$z = d + d_{ss}, \quad -k_2\frac{\partial T_2}{\partial z} = h_b(T_2 - T_\infty) + \varepsilon^-_{ss}\sigma(T_2^4 - T_\infty^4)$$

Initially the temperature is T_∞ everywhere. The thermophysical properties in Equation 1 have to be averaged over the two materials. The laser beam energy that is absorbed by the silicon layer is given by [17]:

$$q_{abs}(x, y, T_1) = \sum_{i=1}^{n_w}\left[1 - R_{\lambda i}(T_1) - \tau_{\lambda i}(T_1)\right] q_{\lambda i}(x, y) \qquad (3)$$

where n_w is the number of laser beam peak wavelengths and $q_{\lambda i}(x, y)$ is the laser light source irradiance distribution. The beam irradiance distribution can be shaped to be elliptical or circular.

The reflectivity $R_{\lambda i}$ and the transmissivity $\tau_{\lambda i}$ in Equation 3 are calculated [17] using thin film optics that take into account wave interference effects in the multilayer thin film structure. When liquid, the silicon film is opaque and its reflectivity at a wavelength of $\lambda = 488$ nm is $R = 0.527$.

The radiation losses from the region 1 was calculated from

$$q_{rad} = \sigma(\varepsilon^+_{cap} + \varepsilon^-_{cap} + \varepsilon^+_{si} + \varepsilon^-_{si})(T_1^4 - T_\infty^4) \qquad (4)$$

The hemispherical total emissivities appearing in this equation were calculated by analyzing the electromagnetic wave propagation through the multilayer structure, which was considered isothermal and in thermal equilibrium with its surroundings. The convection heat loss in Equation 1 is given by

$$q_{cv} = h_t(T_1 - T_\infty) \qquad (5)$$

The heat transfer coefficients h_t and h_b are estimated using expressions for free convection from horizontal surfaces. The radiation and the convective losses are very small compared to the laser light absorption in the semiconductor layer. The length scale in this problem is small so that conduction is the dominant mode of heat transfer. On the other hand, liquid silicon is opaque to radiation, exhibiting a metallic behavior. The complete radiative transfer equation does not need to be solved in the multilayer structure as is the case in the large scale vertical Bridgman system for bulk silicon crystal growth [19].

The enthalpy of the lumped material per unit

volume can be written in terms of the enthalpies of its constituents

$$e_l = \frac{e_{cap} d_{cap} + e_{si} d_{si}}{d} \qquad (6)$$

No phase change is considered for the capping SiO_2 layer during the entire process, and its volumetric heat capacity can be assumed constant:

$$e_{cap} = \int_{T_m}^{T} (\rho c_p)_{cap} dT = (\rho C_p)_{cap} (T - T_m) \qquad (7)$$

For an element of the silicon film completely in solid or liquid phase, we have

$$e_s = \int_{T_m}^{T} (\rho c_p)_s dT \qquad (8a)$$

$$e_l = \int_{T_m}^{T} (\rho c_p)_{si} dT + L \qquad (8b)$$

If the element of the silicon film contains both phases, an average enthalpy may be defined as

$$e_{si} = f e_l + (1-f) e_s \qquad (8c)$$

Where f is the volumetric fraction of the element in the liquid phase. By using an average value for the element containing the solid-liquid interface and employing Equations 8a and b in Equation 8c the following expression is obtained

$$e_{si} = fL + (\rho c_p)_{av} (T - T_m) \qquad (8d)$$

By substitution for e_{cap} and e_{si} in Equation 6 from Equation 7 and Equations 8 (a,b,c,d), a relation between the enthalpy and temprature of a grid point in the lumped region is derived.

The enthalpy formulation is used in the phase change zone of the lumped layers. The left hand side of Equation 1 is written in terms of enthalpy to give.

$$\frac{\partial e_l}{\partial t} + V \frac{\partial e_l}{\partial x} = \frac{\partial}{\partial x}\left(k_l \frac{\partial T_l}{\partial x}\right) + \frac{\partial}{\partial y}\left(k_l \frac{\partial T_l}{\partial y}\right) + \frac{q_{abs} - (q_{md} + q_{cv} + q_{cd})}{d} \qquad (9)$$

Equation 9 is used for each discretized spatial domain regardless of whether the domain is in solid or liquid state or contains both phases. Appropriate average values must be used for the thermophysical properties in Equation 9. The solid-liquid interface location is a function of x,y, and t. At any point on the interface the following conditions apply [20].

$$T_s = T_l = T_m \qquad (10)$$

$$\left[1 + \left(\frac{\partial Y_s}{\partial x}\right)^2\right]\left[k_s \frac{\partial T_s}{\partial y} - k_l \frac{\partial T_l}{\partial y}\right] = L \frac{\partial Y_s}{\partial t} \qquad (11)$$

$$\left[1 + \left(\frac{\partial X_s}{\partial y}\right)^2\right]\left[k_s \frac{\partial T_s}{\partial x} - k_l \frac{\partial T_l}{\partial x}\right] = L\left(\frac{\partial X_s}{\partial t} - V\right) \qquad (12)$$

where $\frac{\partial Y_s}{\partial t}$ and $\frac{\partial X_s}{\partial t}$ are the velocity components of the interface in the y and x directions respectively.

NUMERICAL METHOD

The computational domain in the x-y plane is divided into the inner region and the outer region. The solid-liquid interface is confined in the inner region. Each region is discretized by using a fixed in time orthogonal mesh. Different sizes of the inner region were used for the different cases examined in this work. For the circular beam intensity profile, the inner region consisted of 21×21 grids located 7 μm apart ($\Delta x_i = \Delta y_i = 7\mu m$), while for the elliptic beam profile 45×15 grids of the same size were used. In the outer

region grid sizes of either $\Delta x_0 = \Delta y_0 = 50\ \mu m$ or $\Delta x_0 = 35\ \mu m$ and $\Delta y_0 = 50\ \mu m$ were used. The mesh is uniform in the z-direction, with the first point placed in the lumped layers and the rest located in the substrate. The grid spacing is sufficient to capture the temperature distribution in the liquid pool and across the phase boundary with reasonable accuracy. The temperature distributions and the position of the moving interface did not change noticeably when the mesh was refined by a factor of two.

Equations 1,2 and 9 were written in explicit finite difference forms. The enthalpy formulation, Equation 9 was only used for the inner region of the lumped layers, where the phase change occurs. For the outer region of the lumped layers the conduction Equation 1 was used. The three-dimensional conduction Equation 2 was used to solve for the temperature distribution in the substrate. Figure 1 shows the volume element (i, j) in the lumped layers containing the interface and its neighboring elements. At time t, the interface S divides the silicon part into a liquid portion ($f \Delta x_i \Delta y_j$) and a solid portion ($(1-f)(\Delta x_i \Delta y_j)$). After a small increment in time, Δt, the interface moves to new location S' resulting in an increase of the liquid protion. The progress of the interface can be caluclated from the finite difference forms of Equations 11 and 12.

If the interface is in the element at the center of the laser beam, the following equation must be used:

$$L\frac{Y_s'(i) - Y_s(i)}{\Delta t} = k_s\frac{T_1(i,j+1) - Tm}{y(j+1) - Y_s(i)} - k_l\frac{Tm\,T_1(i,j)}{Y_s(i)} \qquad (13)$$

This equation assumes radial symmetry for the interface as long as its diameter is less than Δxi. At the beginning of melting, when $Y_s(i) = 0$, the last term of Equation 13 becomes infinite. This singularity can be removed by writing Equation 13 in a backward time difference form. Therefore for the starting conditions at the begining of melting:

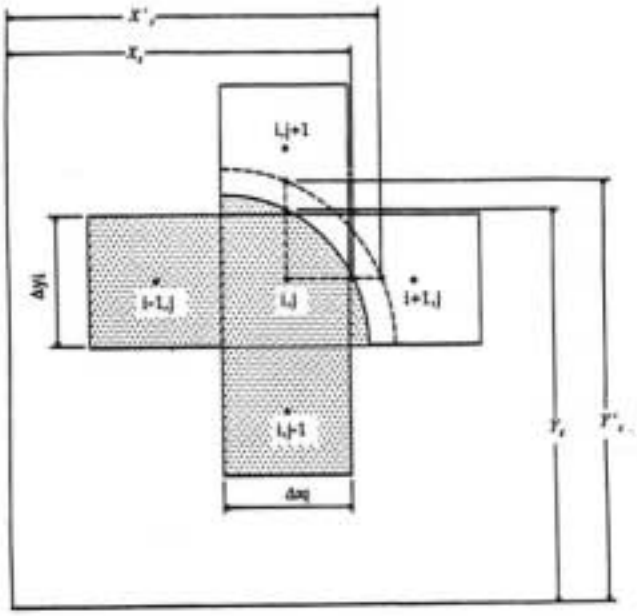

Figure 1. Progress of solid-liquid interface during time Δt.

$$L\frac{Y_s'(i)}{\Delta t} = k_s\frac{T_1'(i,j+1) - Tm}{y(j+1) - Y_s'(i)} - k_l\frac{Tm - T_1'(i,j)}{Y_s'(i)} \qquad (14)$$

Using Equations 6,7 and 8, Equation. 14 may be written as:

$$L\frac{Y_s'(i)}{\Delta t} = k_s\frac{T_1'(i,j+1) - Tm}{y(j+1) - Y_s'(i)} + \frac{k_l}{(\rho c_p)_l}\,\frac{e_j'(i,j) - \pi\left(\frac{Y_s'(i)}{\Delta y_i}\right)^2 L\frac{d_{si}}{d}}{Y_s'(i)} \qquad (15)$$

For the circular symmetric case, the computational domain is only one quarter of the physical domain, with the xz and yz planes considered adiabatic. If elliptic symmetry exists, one half of the physical domain needs to be considered, with the xz plane being adiabatic.

RESULTS AND DISCUSSION

The calculations were carried out for a range of laser beam parameters. It was assumed that the CW laser beam is turned on instantaneously and that it is focused on the silicon film. The results for the tem-

perature distributions in the silicon film and the substrate and size of the molten pool are presented as functions of time. The laser beam power was varied from P_T= 1.0 to 1.8 W and the beam radius corresponding to 1/e intensity, $W_{\lambda b}$, was varied from 30 to 80 μm. The results have shown that after an elapsed time of 20 ms, a quasi-steady temperature distribution and melt pool size are virtually established.

Figure 2 shows the temperature rise in a nonmoving silicon film, at the center of the laser beam for beam radii of 30, 40, 50, 60, 70, and 80 μm and total power of 1.8 W. The rate of the temperature increase is remarkably reduced after the beginning of melting. The change in the temperature rise after the intiation of phase change is due to a larger thermal conductivity of liquid silicon than that of the solid at the melting temperature. It is also caused by a drop in the absorption of the silicon film by almost 40 percent as a result of phase change to liquid. Figure 2 shows that for $W_{\lambda b}$= 30 μm, the silicon temperature at the center reaches the boiling point, T= 2628K, within 5ms. This is related to the "Keyhole" formation observed in the experiments [17]. The numerical scheme does not account for this effect. Figure 3 shows the melt pool size for the same parameters as in Figure 2. As

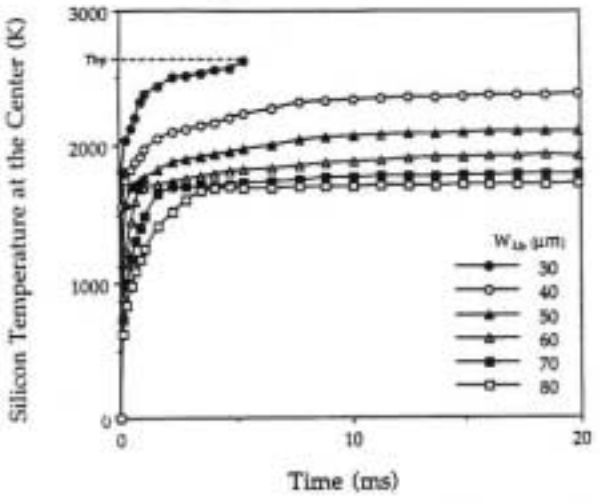

Figure 2. Silicon temperature at the center of the laser beam for P_T= 1.8 W, $W_{\lambda b}$= 30,40,50,70 and 80 μm and V= 0 mm/sec.

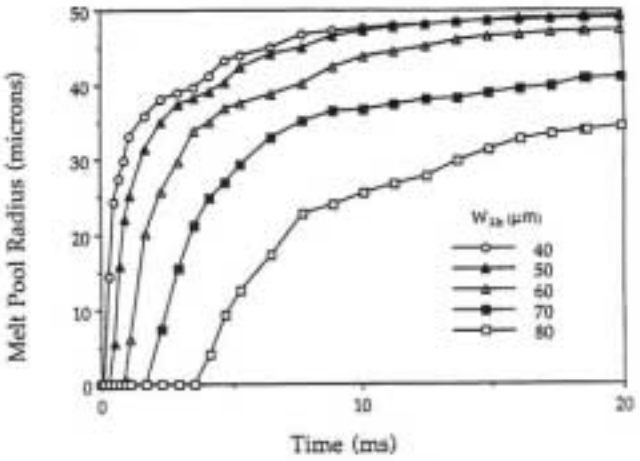

Figure 3. Melt pool rodius in the silicon film for P_T= 1.8 W, $W_{\lambda b}$= 40,50,60,70, and 80 μm and V= 0 mm/sec.

the beam radius is increased the beginning of melting is delayed.

Figure 4 shows the melt pool size as a function of the laser beam radius for different total powers. The melt radius rises to a maximum with respect to $W_{\lambda b}$, and decreases to zero at a larger beam radius. For a small radius the energy intensity is sufficient to cause a "keyhole" over the entire beam waist shortly after the laser goes on. On the other hand, for very large beam radii, the energy intensity would not be sufficient to cause melting. Therefore, for a given total power, there is a beam waist for which the

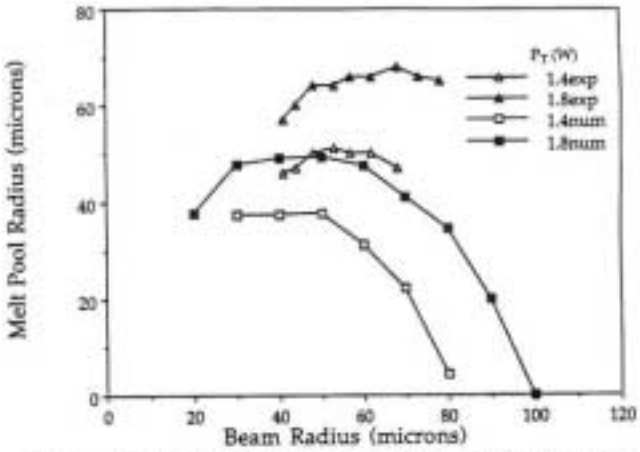

Figure 4. Experimental data and numerical results for the quasi-steady melt pool radius for P_T= 1.8 and 1.4 W; t= 20 msec, and V= 0 mm/sec.

energy intensity distribution is such that the largest pool is created. Also shown in Figure 4, are the experimental results [17] for the same beam parameters. It can be stated that the numerical model captures the experimental trends. The differences between the numerical results and the experimental data become larger at small and large radii. For P_T= 1.8 W and $W_{1/e}$= 30 μm, the silicon temperature at the center of the laser beam reaches the boiling point in 5 ms. On the other hand, at the larger beam diameters the decrease of the pool size is not significant as shown by the experimental results; instead partial melting is observed. The partially molten zone contains liquid coexisting with solid filaments. The present numerical scheme does not address this phenomenon, since it assumes that the molten zone contains only the uniformly liquid phase. Computational models of partially molten, mushy zones generated by internal radiative absorption in semitransparent materials have been reported [21]. It is noted that in thin semiconductor film laser melting the problem would require treatment of the different material optical properties by the solid and liquid phases and light absorption within the partially molten zone.

Figure 2 shows that for P_T= 1.8 W, and $W_{1/e}$= 80 μm the peak silicon layer temperature does not substantially exceed the melting point. As the temperature gradients across the solid-liquid interface decreases, the phase change boundary may become unstable with respect to temperature field perturbations. These instabilities are surface tension limited and may give rise to solid-liquid coexistence [22]. The difference between the experimental data and the numerical results may be due to departures of the thin film thermal and optical properties from the bulk form values. For instance, the thermal conductivity of micron-thick silicon films may be several times smaller than the bulk silicon value which was used in the calculations.

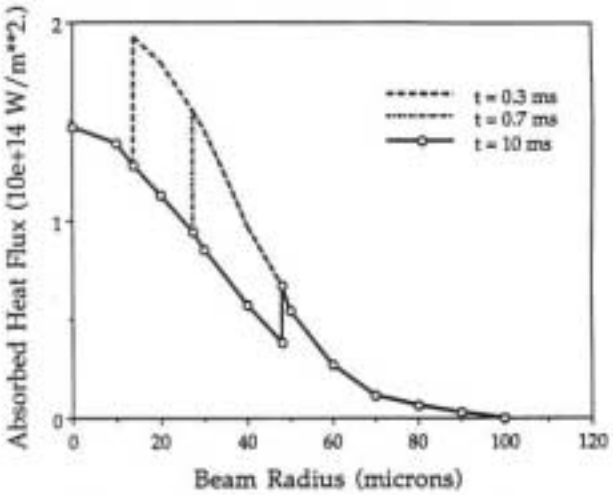

Figure 5. Radial distribution of the absorbed energy flux at t= 0.3, 0.7, and 10 msec for P_T= 1.8 W, and $W_{1/e}$= 40 μm, and V= 0 mm/sec.

Figure 5 shows the absorbed energy intensity profiles at different times. The total power is 1.8 W and the beam radius is 40 microns. The absorbed energy decreases following a Gaussian type profile up to the solid-liquid interface. At the interface the energy increases sharply due to a larger absorpivity of the solid silicon than that of the liquid. Then the energy distribution follows the exponential variation of the laser beam.

Figure 6 shows the melt pool for $W_{1/e}$= 53 μm and a sample translational speed, V= 2mm/sec. At V=

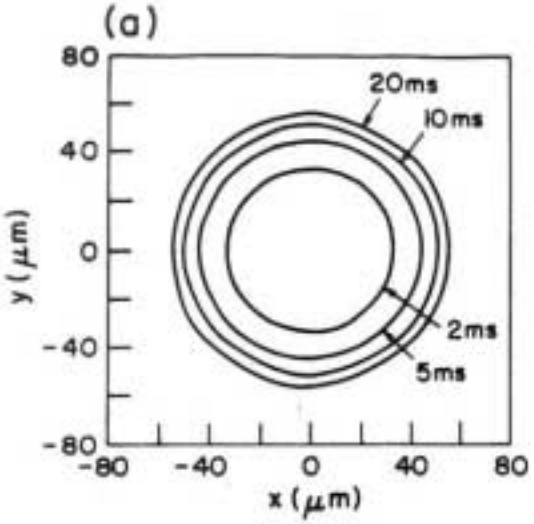

Figure 6. Melt pool in the silicon film for P_T= 1.8 W, $W_{1/e}$= 53 μm at t= 2,5,10,20 msecs; V= 2 mm/sec.

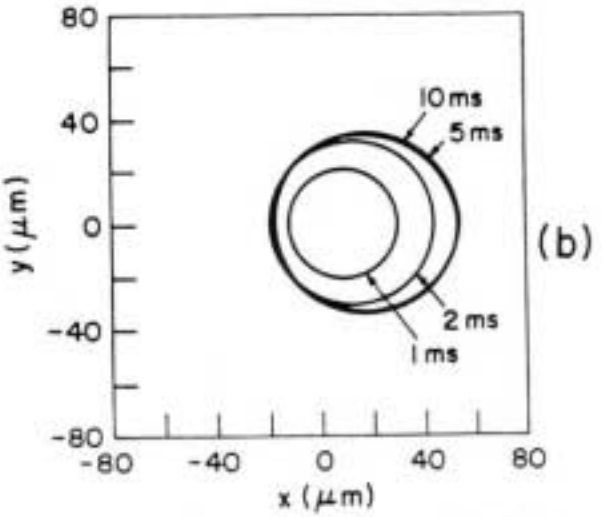

Figure 7. Melt pool in the silicon film for P_T= 1.8 W, $W_{1/e}$= 53 μm at t= 1,2,5,10, msecs; V= 20 mm/sec.

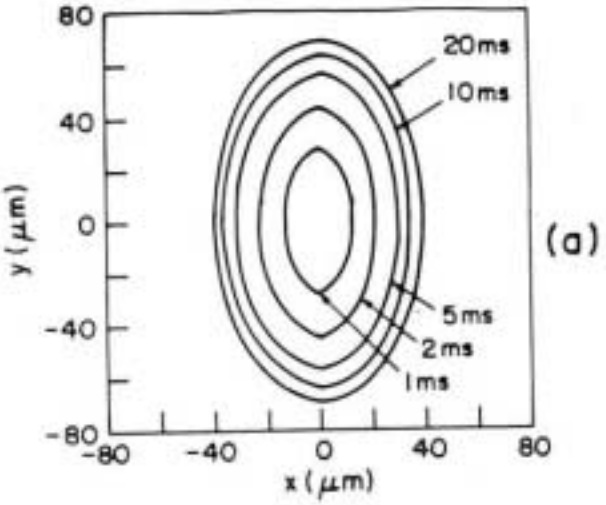

Figure 8. Melt pool in the silicon film for P_T = 1.8 W, $W_{1/e}$= 36 μm, W_{1/e^2}= 76 μm, at t= 1,2,5,10,20, msec; V= 2 mm/sec.

2mm/sec the shape of the pool is only slightly distorted due to the effect of the translational speed of the target material. The calculated diameter in the x-direction is 112.4μm and the diameter in the y-direction is 110.6 μm. The experimental value of the average molten pool diameter was 199 μm[17], indicating a relatively good agreement between the numerical and experimental results. Figure 7 shows the melt pool size for the same laser beam parameters at V=20mm/sec. As the translational speed is increased, the melt pool becomes smaller.The shrinkage of the molten pool at higher translational speeds may be explained in the following manner. When the laser beam is applied on the surface of the target, a melt pool will be created if the laser beam power is sufficient. If the relative translational speed between the target and the heat source is zero, increasing portion of the incident energy is accumulated in the pool, thereby increasing the melt pool diameter until a quasi-static state is reached. Howevere, if the relative translational speed is not zero, the high intensity portion of the source will be convected away from the initially created melt pool, resulting in a smaller pool size. In this case more energy is stored in the tartet material as sensible heat rather than latent heat as compared to the zero speed case. The molten pool movement in the x-direction is still very small for the speed of about 5 mm/sec, but becomes quite noticeable for the higher speeds.

Figure 8 shows the melt pool size for a laser beam with elliptic intensity distribution. The calculated lengths of the major and minor axes of the elliptically shpaed molten pool along the x- and y-directions, at t= 20 msec, are 144 and 80 μm respectively. The corresponding experimental values are 166 and 78

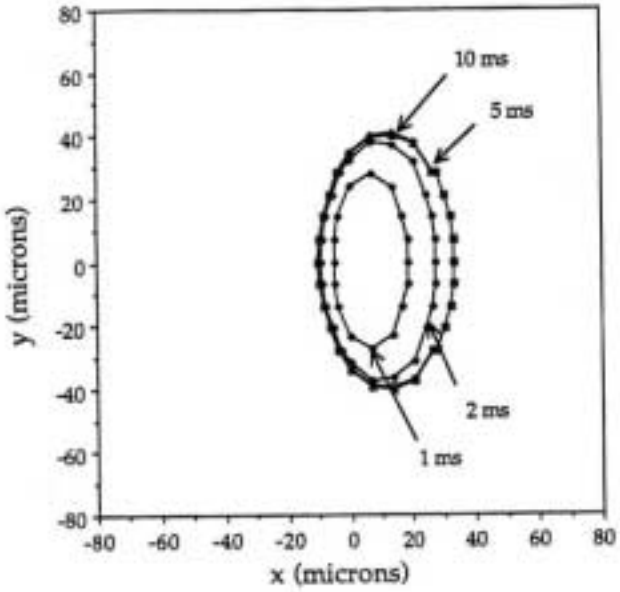

Figure 9. Melt pool in the silicon film for P_T= 1.8 W, $W_{1/e}$= 22 μm, W_{1/e^2}= 100 μm, at t= 1,2,5,10,20, msec; V= 40 mm/sec.

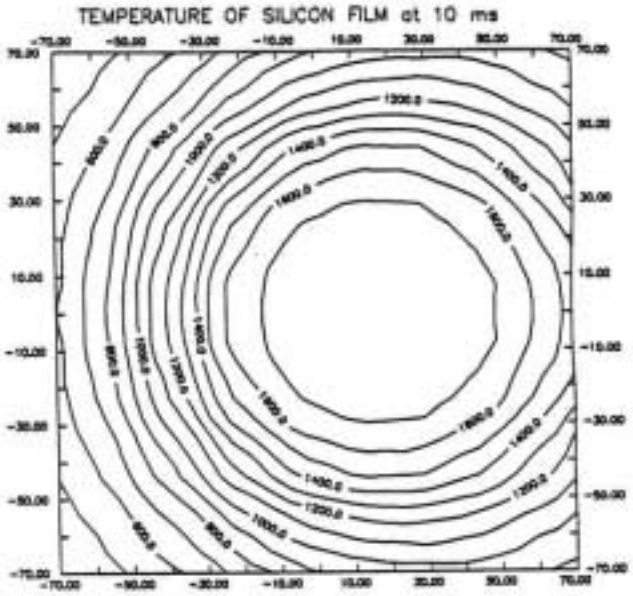

Figure 10. Contour plot of the temperature filed in the silicon layer at t= 10 msec, for P_T= 1.8 W, $W_{\lambda b}$= 53 μm, V= 40 mm/sec.

μm [17]. Relatively good agreement between experimental and theoretical results is confirmed. Figures 9 shows the melt pool growth for the same elliptic laser beam parameters, and for V= 40 mm/sec. It is noted that an increase in the translational speed results in a smaller melt pool size, a shorter time required to reach steady state melt pool size, and a more pronounced distortion of the molten pool shape.

Figure 10 shows a contour plot of the temperature in a silicon film moving at a speed of V= 40 mm/sec, irradiated by a laser beam of circular shapes with P_T= 1.8 W, $W_{\lambda b}$= 53 μm, at t= 10 msec. An elliptically shaped laser beam with $W_{\lambda b}$= 22 μm, $W_{\lambda b}$= 100 μm generates the temperature filed shown in Figure 11.

CONCLUSIONS

The three-dimensional heat transfer problem involving melting a silicon film on top of a glass substrate was studied. The target was irradiated by a moving laser beam of specified temporal and spatial distributions of intensity. The temperature distribution and the size of melt pool in the film were calculated for a

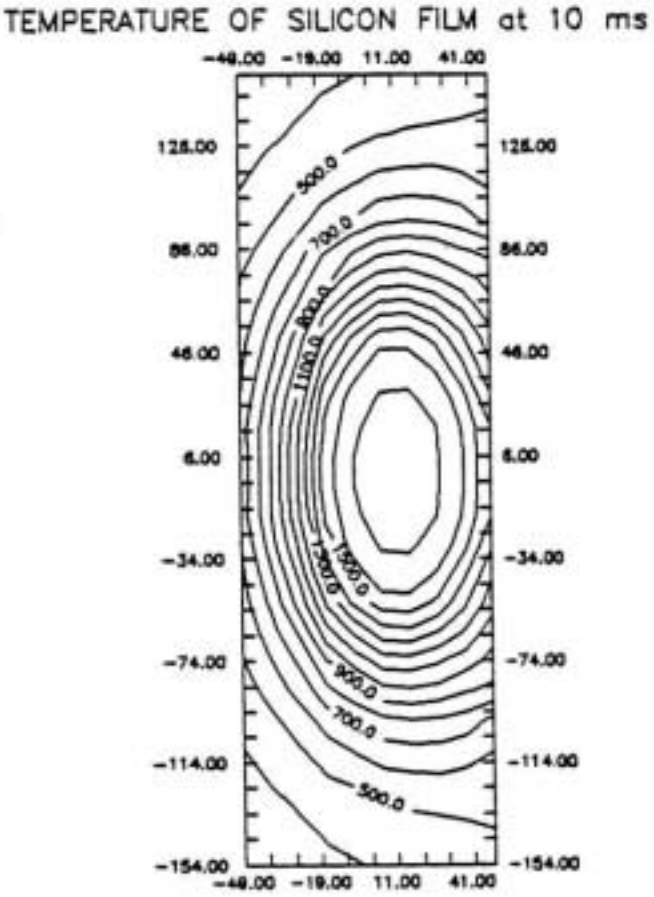

Figure 11. Contour plot of the temperature filed in the silicon layer at t= 10 msec, for P_T= 1.8 W, $W_{\lambda b}$= 36 μm, V= 40 mm/sec.

range of beam parameters. The effects of the translational velocity of the beam on the shape and size of the melt pool as well as the isotherms were investigated.

ACKNOWLEDGEMENT

Support to this work by the National Science Foundation, under Grant CTS-9096253 is gratefully acknowledged. The help of Scott Taylor and Hee Kuwon Park of the Department of Mechanical Engineering at the University of California at Berkeley is appreciated.

NOMENCLATURE

C_p= specific heat

$d = d_{cap} + d_{si}$

d_{cap}= encapsulating layer thickness

d_{si}= silicon film thickness

d_{ss}= substrate thickness

e= enthalpy per unit volume

f= liquid volume fraction

h_b= heat transfer coefficient at the bottom surface

h_t= heat transfer coefficient at the top surface

i= numbering for grid points in x direction

j= numbering for grid points in y direction

k= thermal conductivity

L= Latent heat of fusion per unit volume

n_w= number of laser beam peak wavelengths

P_T= total power of laser beam

q_{abs}= absorbed heat flux

q_{cd}= conduction heat loss

q_{cv}= convection heat loss

q= laser light source irradiance distribution

$q^o_{0,i}$ = peak power intensity of the laser beam

R_{si}= reflectivity

t= time

T= temperature

T_{bp}= boiling point of silicon

T_m= melting point of silicon

T_∞= initial and ambient temperature

V= velocity of target in x-direction

x = coordinate in the scanning direction

X_s= x-coordinate of the solid-liquid interface

y = coordinate in the transverse direction

Y_s= y-coordinate of the solid-liquid interface

Greek letters

ε = emissivity

λ= wavelength

ρ= density

σ= Stefan-Boltzmann constant

τ= transmissivity

Subscripts

cap= encapsulating layer

i= inner region

l= liquid silicon

o= outer region

s= solid silicon

si= silicon

ss= substrate

1= region of lumped layers

2= substrate region

λ = wavelength

Superscripts

+ = emissive loss towards the top

- = emissive loss towards the bottom

′ = value at the new time

REFERENCES

1. G. K. Celler, "Laser Recrystallization of Thin Films on Amorphous Insulating Substrates," *J. Crystal Growth*, Vol. 63, (1983), pp. 429-444.
2. B.Y. Tsaur, "Assessment of Silicon on Insulator Technologies for VLSI," Proceedings, Materials Research Society, A. Chiang et al., MRS, pittsburgh, PA, Vol. 53, (1986), pp. 365-373.
3. J. C. C. Fan, B.Y. Tsaur and M.W. Geis,"Graphite-strip-Heater Zone Melting Recrystallization of Si films," *J. Crystal Growth*, Vol. 63, (1983), pp. 453-483.
4. S. Kawamura, et al., "Recrystallization of Si on Amorphous Substrates by Doughnut-Shaped CW Ar Laser Beams," *Appl. Phys. Lett.*, Vol. 40, No. 5, (1982), pp. 394-395.
5. T. J. Stultz and J. F. Gibbons, "The Use of Beam Shaping to Achieve Large-Grain CW Laser-Recrystallized Polysilicon Amorphous Substrates," *Appl. Phys. Lett.*, Vol. 39, No.6, (1981), pp. 498-500.
6. J. R. Ockendon and W. R. Hodgkins, (eds.), "Moving Boundary Problems in Heat Flow and Diffusion", Oxford University Press, Oxford, (1975).
7. V. Lundardini, "Heat Transfer in Cold Climates", Van Nostrand Reinhold, New York, (1981).

8. N. Shamsundar, "Department of Mechanical Engineering", Ph.D. Thesis, University of Minnesota, Minnesota, (1975).

9. M. Salcudean and Z. Abdullah, "On Numerical Modeling of Heat Transfer During Solidification Process." *Int. J. Num. Met. in Eng.*, 25. (1988), pp. 445-473.

10. S. A. Kokorowski, G. L. Olson and L. D. Hess, "Thermal Analysis of CW laser Annealing beyond the Melt Temperature, "Proceedings, Material Research Society, J.F. Gibbons et al., MRS, North-Holland, NY, Vol. 1, (1981), pp. 139-146.

11. P. Schvan and R. E. Thomas, "Time Dependent Heat Flow Calculation of CW Laser-Induced Melting of Silicon," *J. Appl. Phys.*, Vol. 57, No. 10, (1985). pp. 4738-4741.

12. K. Kubota, C. E. Hunt and J. Frey, "Thermal Profiles Durnig Recrystallization of the Silicon Insulator with Scanning Incoherent Light Line Sources," *Appl. Phys. Lett.*, Vol. 46, No. 12, (1986), pp. 139-146.

13. I. N. Miaoulis and B. B. Mikic, "Heat Source Power Requirements for High Quality Recrystallization of Thin Silicon Films on Electronic Devices," *J. Appl. Phys.*, Vol. 59, No. 5, (1986), pp. 1658-1666.

14. C. P. Grigoropoulos, R. H. Buckholz and G. A Domoto, "A Heat Transfer Algorithm for the Laser Induced Melting and Recrystallization of Thin Silicon Layers," *J. Appl. Phys.*, Vol. 60, No. 7, (1986), pp. 2304-2309.

15. D. R. Atthey, "A Finite Difference Scheme for Melting Problems," *J. Inst. Math Aplics.*, Vol. 13, (1974), pp. 353-365.

16. N. Shamsundar and E. M. Sparrow, "Analysis of Multidimensional Conduction Phase Change via the Enthalpy Model," *ASME Journal of Heat Transfer*, Vol. 98, (1975), pp. 551-557.

17. C. P. Grigoropoulos, W. E. Dutcher and A. F. Emery, "Experimental and Computational Analysis of Laser Melting of Thin Silicon Films," *ASME Journal of Heat Transfer*, Vol. 113, (1991), pp. 21-29.

18. A. A. Rostami, R. Greif and E. R. Russo, "Modified Enthalpy Method Applied to Rapid Melting and Solidificantion," *Int. J. Heat Mass Transfer*, Vol. 35, No. 9, (1992). pp. 2161-2172.

19. H. Matsushima and R. Viskanta, "Effects of Internal Radiative Transfer on Natural Convection and Heat Transfer in a Vertical Crystal Growth Configuration," *Int. J. Heat Mass Transfer*, Vol. 4, (1990), pp. 1957-1968.

20. M. N. Ozisik, "Heat Conduction", John Wiley and Sons, (1980), pp. 397-438.

21. S. H. Chan, D. H. Cho and G. Kogamus Tafaogullari, "Melting and Solidification with Internal Radiative Transfer- A Generalized Phase Change Model", *Int. J. Heat Mass Transfer*, Vol. 26, No. 4, (1983), pp. 621-633.

22. C. P. Grigoropoulos, R. H. Buckholz and G. A. Domoto, "A Thermal Instability in the Laser-Driven Melting and Recrystallization of Thin Silicon Films on Glass Substrates,"*ASME Journal of Heat Transfer*, Vol. 109, (1987), pp. 841-846.

23. Y. C. Tai, C. H. Mastrangelo and R. S. Muller, "Thermal Conductivity of Heavily Doped Low-Pressure Chemical Vapor Deposited Polycrystalline Silicon Films," *J. Appl. Phys.*, Vol. 63, (1988), pp. 1442-1447.